Modelling microbial transport in simulated low-grade heap bioleaching systems: the hydrodynamic dispersion model

Elaine Govender[1,a,*], Athanasios Kotsiopoulos[1,b], Christopher G. Bryan[2,c] and Susan T. L. Harrison[1,d]

[1] Centre for Bioprocess Engineering Research (CeBER), Department of Chemical Engineering, University of Cape Town, Rondebosch 7701, South Africa.

[2] Present address: Environment and Sustainability Institute, University of Exeter, Penryn Campus, Penryn, TR10 9FE, UK.

[a] Elaine.Govender@uct.ac.za, [b] Athanasios.Kotsiopoulos@uct.ac.za, [c] C.G.Bryan@exeter.ac.uk, [d] Sue.Harrison@uct.ac.za,

*Corresponding author: +27 21 650 1872

Abstract

The hydrodynamic model was developed to describe microbial growth kinetics within heap bioleaching systems. Microbial partitioning between the bulk flowing pregnant leach solution (PLS) and ore-associated phases that exist within the low-grade chalcopyrite ore bed, as a function of microbial transport between these identified phases, was investigated. Microbial transport between the bulk flowing PLS and ore-associated phases was postulated to be driven by the microbial concentration gradient between the phases, with advection and dispersion forces facilitating microbial colonisation of, and transport through, the ore bed. The population balance model (PBM) was incorporated into the hydrodynamic model to estimate mineral dissolution rates as a function of available surface area appropriately. Temporal and spatial variations in microbial concentration in the PLS and ore-associated phases are presented together with model predictions for overall ferrous and ferric iron concentrations, which account for iron concentrations in the bulk flowing PLS and that in the vicinity of the mineral surface. The model predictions for PLS and ore-associated microbial concentrations are validated with experimental data, demonstrating the improvement of this model over the previously presented 'biomass model'. Based on Michaelis-Menten type kinetics, model-predicted *true* maximum specific growth rates for *Acidithiobacillus ferrooxidans* in the PLS and ore-associated phases were found to be 0.0004 and 0.019 h^{-1}, respectively. Estimated microbial attachment and detachment rates suggest that microbial growth is more prolific in the ore-associated phases with subsequent transport to the bulk flowing PLS. Sensitivity analysis of the hydrodynamic transport model to changes in the advection mass transfer coefficient, dispersion coefficient and inoculum size are discussed. For the current reactor configuration, increasing the irrigation rate from 2 to 2.5 L m^{-2} h^{-1}, i.e. increasing the advection mass transfer rate, resulted in a significant decrease in microbial retention within the ore bed.

Keywords: heap bioleaching; unsaturated packed beds; microbial colonisation; microbial transport rates; microbial growth rates; microbial modelling

1. Introduction

Heap bioleaching is considered a feasible technology for the extraction of base metals from low-grade mineral sulphide ores. Research is currently focussed on understanding the sub-processes governing the dissolution of low-grade copper-bearing ores in heaps. Chalcopyrite is thought to be the most abundant and refractory copper-bearing mineral resource (Wang, 2005, Watling, 2006). However, lower mineral sulphide dissolution rates have been observed in commercial heaps (Chen and Wen, 2013, Panda et al., 2012, Watling, 2006) than previously obtained in tank bioleaching systems at temperatures exceeding 50°C (Batty and Rorke, 2006) and pilot scale heaps (Dew et al., 2011), as a result of poor temperature progression within the heap which limits efficacy.

In the dissolution of chalcopyrite, both ferric iron and hydronium ions react with the mineral sulphide, as in Eqs. 1 and 2, respectively. Studies have shown that these reactions together with the microbial oxidation of ferrous iron (Eq. 3), determine the ferric to ferrous iron ratio which, in turn, affects the rate of chalcopyrite dissolution (Córdoba et al., 2008, Hiroyoshi et al., 2008). In addition, the microbial oxidation of reduced sulphur species regenerates the hydronium ions (Eq. 4) responsible for maintaining low pH conditions necessary for both optimum microbial oxidation and the prevention of iron precipitation.

$$CuFeS_2 + 4\,Fe^{3+} \rightarrow Cu^{2+} + 5\,Fe^{2+} + 2\,S^0 \quad (1)$$

$$CuFeS_2 + 4\,H^+ + O_2 \rightarrow Cu^{2+} + Fe^{2+} + 2\,S^0 + 2\,H_2O \quad (2)$$

$$4\,Fe^{2+} + 4\,H^+ + O_2 \xrightarrow{iron\ oxidiser} 4\,Fe^{3+} + 2\,H_2O \quad (3)$$

$$2\,S^0 + 3\,O_2 + 2\,H_2O \xrightarrow{sulphur\ oxidiser} 2\,SO_4^{2-} + 4\,H^+ \quad (4)$$

Although dump bioleaching has been applied successfully for the treatment of low-grade, copper-bearing ores, previous studies have demonstrated the significance of variation in temperature, oxygen concentration, concentration of chemical species, microbial activity and abundance across the length and depth of test scale dumps (Bhappu et al., 1969, Murr, 1980, Murr and Brierley, 1978). Heap bioleaching has begun to replace dump bioleaching as the more feasible technology (Chen and Wen, 2013, Norgate and Jahanshahi, 2010, Watling, 2006); however, the copper inventory within the heap

often requires months before metal recovery can occur. Decreasing the holdup of this copper inventory has significant potential benefit to the industry.

Typically, commercial heap operations experience long heap start-up periods during which microbial activity is low, leading to slow temperature progression within the heap and low mineral dissolution rates. Energy loss from the heap during start-up may be minimised through effective management of the solution irrigation rate and aeration of the heap (Dixon, 2000, Lizama, 2001, Muñoz et al., 1995). The exothermic sulphide mineral dissolution reactions which generate energy within the heap are controlled by the availability of chemical and microbial species, distributed within the heap by the bulk flowing liquid stream as well as the degree of liberation and accessibility of the sulphide mineral. Escobar et al. (1996) and van Loosdrecht et al. (1990) suggested that in a mineral leaching environment, bioleaching micro-organisms may be concentrated in the phases associated with the mineral.

Recent studies have demonstrated that bioleaching micro-organisms are present distributed non-uniformly across the identified phases within the heap; namely, in the bulk flowing pregnant leach solution (PLS), in the stagnant interstitial solution, and weakly and strongly attached to the mineral surface (Chiume et al., 2012, Govender et al., 2013, Tupikina et al., 2014). These authors found that the growth of *At. ferrooxidans* in the PLS did not represent that in the stagnant interstitial solution and attached phases, with microbial abundance in the ore-associated phases (interstitial and attached) at least two to three orders of magnitude greater than that in the PLS. In the study by Govender et al. (2013), maximum specific growth rates in the PLS, interstitial and ore-attached phases were estimated assuming no microbial transport between the identified phases. The authors concluded that the specific growth rates in the PLS were exaggerated by the transport of micro-organisms from the ore-associated phases to the bulk flowing solution and may therefore be regarded as *apparent* maximum specific growth rates. The estimation of *true* maximum specific microbial growth rates in whole ore leaching systems, therefore, requires accounting for microbial transport between the phases.

Previously, van Loosdrecht et al. (1990) proposed that a portion of new microbes grown in the reversibly attached population may leave the vicinity of the mineral surface. The transport mechanisms employed by micro-organisms to travel short distances, namely chemotaxis, Brownian motion, attraction by electrostatic forces and hydrophobicity, are only effective at the micrometer scale (Rossi, 1990). The conceptual understanding of microbial transport in mineral bioleaching systems, as presented by van Loosdrecht et al. (1990) and Rossi (1990), was built on the work of Marshall (1976), who interpreted numerous studies on porous soil systems aimed at pathogen removal for the remediation of soils.

Expanding on the postulations by Marshall (1976), the advection-dispersion equation has been used to model spatial and temporal variations in microbial concentration in both saturated and unsaturated, porous soil systems (Tan et al., 1994, Taylor and Jaffé, 1990, Tufenkji, 2007). However, few studies have modelled microbial transport in heap bioleaching systems (Leahy et al., 2004, Neuburg et al., 1991, Petersen and Dixon, 2003). None of these cited studies have supported model predictions with experimental validation of microbial population dynamics and growth in the ore-associated phases. In addition, microbial transport from the bulk flowing solution to the solid medium was typically modelled assuming either irreversible attachment, with no detachment term, or reversible attachment described by equilibrium or kinetic terms. In each of the previous heap leaching models, microbial transport was assumed to be governed by an advection-dispersion equation with microbial growth, attachment, detachment and death rates described by a single empirical source/sink term. Although these studies have acknowledged the microbial transport phenomena present in heaps, none have decoupled the effect of transport on *true* microbial growth rates in the identified phases. Additionally, the dynamic nature of the microbial community has not been described.

Recently, Soto-Rojo et al. (2013) presented a model to simulate microbial abundance and activity within sequential lifts in a commercial heap as a function of physico-chemical conditions. The proposed model was aimed at predicting the spatial variation in microbial population dynamics between adjacent lifts, based on correlations obtained from pattern recognition in large data sets. However, the authors obtained poor correlations (R^2 values between 0.53 and 0.71) in predicted microbial abundance as model validation was based on the assumption that microbial abundance, growth and activity in the PLS was representative of that within all phases in the heap.

This study builds on the findings of the biomass transport model presented previously in Govender et al. (2014). The model was developed to validate the hypothesis that the driving force for microbial transport between the PLS and ore-associated phases was largely due to the microbial concentration gradients across the associated boundaries. Although the biomass model successfully predicted the temporal variation in microbial abundance in the PLS and ore-associated phases, the microbial transport rates between the phases were poorly estimated.

The current paper presents the development and validation of an improved mathematical model to predict the microbial population dynamics within a simulated heap bioleaching environment. The model is based on the advection-dispersion equation and describes the growth of *At. ferrooxidans* in the PLS and ore-associated phases as a function of the physical parameters of the solution, ferric and ferrous iron transport through the ore bed and microbial attachment and detachment. It builds on the 'biomass' model reported previously (Govender et al. 2014) to include microbial transport between the PLS and ore-associated phases as a function of the dispersive and advective properties of the bulk

solution. This microbial transport was assumed to be governed by the microbial concentration gradient between these phases and the availability of ferrous iron at the ore surface, as described by the population balance model.

2. Methodology

The experimental system used in this study consisted of multiple, agglomerate-scale mini-column reactors (Govender et al., 2015b). Each mini-column reactor was loaded with *ca*. 150 g of agglomerated ore sample comprised of 4 wt. % pyrite, 0.5 wt. % chalcopyrite, 0.3 wt. % covellite, 0.2 wt. % chalcocite and 0.1 wt. % each of bornite and enargite, together with quartz (44.8 wt.%) and muscovite (28.6 wt.%) as the major gangue minerals . Each ore sample was re-constructed with identical particle size distribution and mass from an acid pre-leached bulk ore sample with 93% passing 16 mm and 12% passing 0.25 mm; the detailed particle size distribution is given by Govender et al. (2015b). A single experiment consisted of multiple mini-column reactors, irrigated from a single feed source and inoculated from the same sample of *At. ferrooxidans* (DSM 14882) culture. Each mini-column reactor, therefore, represented a grab sample of a larger heap. The *At. ferrooxidans* culture was grown on sterile autotrophic basal salts (ABS) medium containing trace elements (Johnson et al., 2008), 0.5 g L^{-1} Fe^{2+} ($FeSO_4.7H_2O$) and 1% (w/v) γ-irradiated pyrite concentrate (< 75μm).

Two sets of tests (A and B), each consisting of one abiotic control and seven biotic mini-column reactors, were inoculated with approximately 10^{10} cells per ton dry ore and run under identical conditions. Sterile feed solution containing 0.2 g L^{-1} Fe^{3+} ($Fe_2(SO_4)_3.xH_2O$), ABS and trace elements at pH 1.7 (96% H_2SO_4) was irrigated over the columns at a rate of 10 mL h^{-1}, equivalent to 2 L m^{-2} h^{-1}. Solution analysis included measurement of pH, redox potential, ferrous and total iron in solution, the latter two using the modified ferric chloride assay described by Govender et al. (2012). Copper in solution was measured by AAS. Details of sampling and analyses are given in Govender et al. (2015b). At specified time intervals, a column from each test was sacrificed and the ore sample analysed for microbial abundance. A column from test A was sacrificed every 72 h, whilst shorter time intervals of 48 h between column sampling was chosen for test B.

For sampling of the ore-associated microbial population, a representative sample of the packed ore bed from the sacrificed mini-column reactor was processed using a standardised detachment protocol (Govender et al., 2013). This method is assumed to result in the extraction of a majority of the ore-associated microbial community. The microbial concentrations in the effluent solution (PLS) and associated with the ore were determined at regular intervals using the Miles-Misra serial dilution

plating protocol (Miles et al., 1938) for the enumeration of viable colony forming units (cfu) on iron overlay plates containing approximately 1.5 g L^{-1} Fe^{2+} ($FeSO_4.7H_2O$) (Johnson, 1995). Variance in quantification of viable cell numbers using the Miles-Misra plating technique was determined by analysing the PLS from multiple columns in an experiment at a single time point and by repeating analysis of cells recovered from a single detached sample. The relative error associated with cell enumeration in columns in the same test was found to be less than 13% (data not shown). A residence time distribution (RTD) study was used to determine the mean residence time, τ, to be 1.45 h. This study, together with compartment models, allowed for an estimation of the volumes of bulk flowing and stagnant solution within the packed bed reactor to be *ca*. 11.7 and 2.3 mL, respectively (Govender et al., 2015b).

The empirical data from tests A and B were presented and discussed previously in Govender et al. (2013) and re-introduced for validation of the biomass transport model (Govender et al., 2014) and the current model.

3. Development of the hydrodynamic dispersion model

At the particle scale, the interstitial phase includes the stagnant liquid boundary between the solid mineral and the bulk flowing solution or PLS. Within this stagnant liquid boundary, the onset of microbial attachment induces the production of extracellular polymeric substances (EPS) which facilitate firm or strong attachment (van Loosdrecht et al., 1990). In a well-functioning heap, aside from the presence of the chemical constituents of EPS, i.e. sugars, lipids and free fatty acids, the concentration of ferric iron in this stagnant solution is proposed to be much greater than that in the PLS (Gehrke et al., 1998, Kinzler et al., 2003, Sand and Gehrke, 2006, Tributsch, 2001). As an experiment progresses, the higher microbial abundance and activity at the mineral surface is expected to result in the rapid turnover of ferrous to ferric iron in this phase, depending on the extent of mineral liberation.

The hydrodynamic dispersion model presented in this study was developed to simulate the effect of solution flow dynamics on the growth and transport of an *At. ferrooxidans* culture within a heap environment. This model aims to describe the transport of chemical and microbial species from the mineral surface across the largely stagnant interstitial phase surrounding the ore particles to the bulk flowing PLS, as a function of dispersion and advection transport phenomena. Although dispersion occurs in all spatial directions, conceptually the model is based on both radial (r-direction) and axial (z-direction) diffusion of solution within the agglomerate-scale column reactor (Figure 1). This was further simplified to account for dispersion in the axial direction only and dispersion in the radial direction was ignored for two reasons: the uniform distribution of leach solution over the top of the

ore bed in the form of a fine mist, and the small height of the ore bed relative to the bed diameter, as described in Govender et al. (2015b).

In this study, the agglomeration of the ore sample and the presence of fine particles was expected to promote the formation of substantial solution hold-up within the ore bed (Bouffard, 2005, Bouffard and West-Sells, 2009, McFarlane et al., 2011). The solution hold-up or stagnant interstitial phase within the heap is constituted of a boundary layer of liquid surrounding individual particles as well as the stagnant solution held up in the void space between individual particles in a cluster forming the agglomerate, as illustrated in Figure 1.

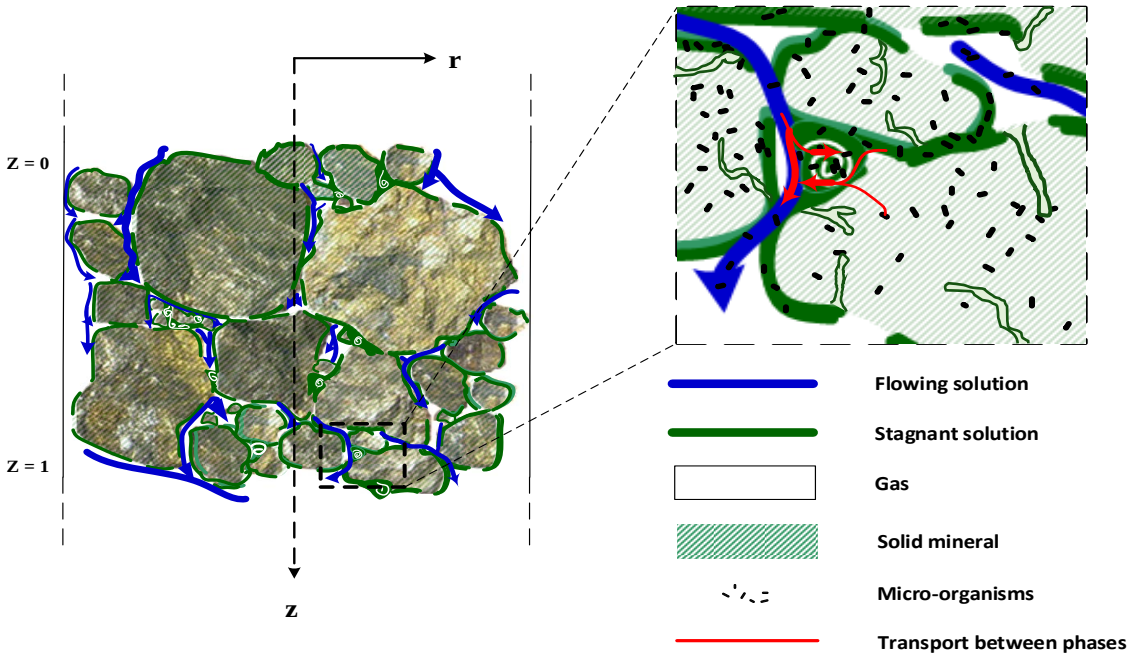

Figure 1: Illustration of the phases that exist within a cluster of particles at the agglomerate scale, describing the interaction between the bulk flowing solution, stagnant interstitial phase, solid mineral surface and gas phases, with radial dispersion in the r-direction and axial dispersion in the z-direction (Govender-Opitz et al., 2016).

In developing the model for microbial transport within a heap, the measured ferric and ferrous iron concentrations in the PLS were proposed to be a poor representation of that in the vicinity of the mineral surface. This assumption was based on the theories postulated by Tributsch (2001) and Sand and Gehrke (2006) whereby the rapid turnover from ferrous to ferric iron near the mineral surface and in the EPS was not described adequately by that measured in the PLS. Thus far, rigorous experimental data supporting this theory has not been reported. Therefore, the overall ferric and ferrous iron balances include the iron concentrations measured in the PLS, $C_{i,PLS}$, and that estimated in the ore-associated phases, $C_{i,ore}$; each normalised with respect to the estimated volumes in each phase (Eq. 5).

$$C_{i,total} \cdot V^R = C_{i,PLS} \cdot V_{PLS} + C_{i,ore} \cdot V_{ore} \quad (5)$$

where C_i is the concentration of the soluble chemical species, either ferric iron, C_{Fe3+}, or ferrous iron, C_{Fe2+}, and V^R, V_{PLS} and V_{ore} are the volumes of total solution in the reactor, bulk flowing PLS and stagnant solutions, respectively. The volumes of PLS and stagnant solution within a mini-column reactor were estimated to be 11.7 and 2.3 mL, respectively (Govender et al., 2015b). These volumes were analysed using compartment model theory from residence time distribution (RTD) curves. The model predictions of overall ferric and ferrous iron concentrations may then be used to infer the ferric and ferrous iron concentrations at the mineral surface, which is expected to be significantly different from that in the bulk flowing solution.

Overall temporal and spatial changes in the ferrous and ferric iron concentrations were predicted using an advection-dispersion equation for solute flow through the heap (Eqs. 6 and 7). The model describes the rate of iron turnover within the ore bed as a function of the rate of mineral dissolution (r^R) and microbial substrate utilisation rate (r_{bio}). Solution-ore contacting results in solute transport out of the ore bed in the bulk flowing PLS *via* axial dispersion and advection mass transfer. The dispersion coefficient constant, D_Z, was estimated from the RTD curves to be 4.24 x 10^{-5} m^2 h^{-1}, using the closed-closed boundary condition assumption. The advection mass transfer coefficient, v, was assumed to remain constant within the ore bed with time, and was determined from the solution irrigation rate of 10 mL h^{-1}, to be 2.46 x 10^{-3} m h^{-1}. Dispersion in the radial direction was assumed to be negligible due to the small volume of the ore bed (ϕ = 80 mm, h = 25 mm) in combination with the uniform distribution of feed solution over the top of the ore bed.

$$\frac{\partial C_{Fe^{3+}}}{\partial t} = D_Z \cdot \frac{\partial^2 C_{Fe^{3+}}}{\partial z^2} - v \cdot \frac{\partial C_{Fe^{3+}}}{\partial z} - 4 \cdot r^R + 4 \cdot r_{bio} \quad (6)$$

$$\frac{\partial C_{Fe^{2+}}}{\partial t} = D_Z \cdot \frac{\partial^2 C_{Fe^{2+}}}{\partial z^2} - v \cdot \frac{\partial C_{Fe^{2+}}}{\partial z} + 5 \cdot r^R - 4 \cdot r_{bio} \quad (7)$$

Stoichiometric coefficients presented in Eqs. 6 and 7 describe the mineral dissolution by ferric iron and microbial ferrous iron oxidation reactions as presented in Eqs. 1 and 3 respectively. Over the period of these experiments, whilst ferrous iron was available in solution for microbial ferrous iron oxidation, the concomitant reactions, i.e. mineral dissolution by acid attack (Eq. 2) and the oxidation of reduced sulphur species by *At. ferrooxidans* (Eq. 4), were assumed to be much slower than the aforementioned reactions (Moinier et al., 2013) and therefore, did not contribute to the corresponding rates of reaction. Initial ferric and ferrous iron concentrations in the feed solution, at t = 0 h and z = 0

m, were sourced from empirical measurements to be 3 mmol Fe^{3+} L^{-1} and 0 mmol Fe^{2+} L^{-1}, while the initial spatial boundary conditions at the bottom of the ore bed were assumed to be negligible.

The application of the advection-dispersion equation to describe the transport of chemical species in unsaturated packed beds simulating heap leaching systems was most recently presented by Ilankoon et al. (2013). In this study, positron emission particle tracking (PEPT) was used to quantify the hydrodynamic dispersion coefficient in the axial (D_z) and radial direction (D_r). Although, the radioactive tracer particles used in the aforementioned study were 400 μm in diameter, which did not represent the flow of dissolved chemical species or micro-organisms in the packed bed, the authors found that the estimation of the D_z using PEPT compared well with that achieved using a salt tracer. No quantitative comparison of dispersion coefficients may be made since empirical estimations are dependent on reactor configuration and irrigation rate, which differ between this study and that by Ilankoon et al. (2013).

. For this study, the intrinsic rate of mineral dissolution was estimated from the ratio of total ferric to total ferrous iron concentration (Hansford and Vargas, 2001) using the rate expression provided in Eq. 8, where k_m is the rate constant [mol m^{-2} h^{-1}] and n is the reaction order of 0.5, as proposed by Williamson and Rimstidt (1994).

$$r''_{mineral} = k_m \cdot \left(\frac{C_{Fe^{3+}}}{C_{Fe^{2+}}}\right)^n \quad (8)$$

However, this approach assumes that all particles in the reactor are of the same size, with equal reaction surface area in contact with the reaction environment over equal exposure times and therefore, contribute equally to the overall mineral dissolution rate. In a system with non-uniform particle size distribution, this assumption results in an over- or under-estimation of the overall mineral leach rate (Kotsiopoulos et al., 2008, Kotsiopoulos et al., 2012). Therefore, the population balance model (PBM) was applied to the current model to better approximate the overall mineral leach rate, r^R [mol m^{-3} h^{-1}], using Eq. 9.

Solution flow dynamics within the mini-column reactors were characterised using RTD studies and demonstrated relatively well-mixed, continuous reactor behaviour (Govender et al., 2015b). Therefore, in the application of the PBM to describe the oxidation of low-grade mineral ores in a heap, a segregation approach was adopted for the modification of the PBM to include both initial particle size distribution, $f_0(l_0)$, and the change in particle reaction surface area with age, $\theta = t_0 - t$ (Kotsiopoulos et al., 2008). The rate contributions for each particle size fraction over a known age range were summed up for the estimation of r^R.

$$r^R = \int_0^\infty \int_0^\infty r''_{mineral}\, A^p(\theta, l_0) \frac{M^p(\theta, l_0)}{V^R}\, \phi_{MS}\, N^T\, f_0(l_0) I(\theta)\, d\theta\, dl_0 \quad (9)$$

In Eq. 9, A^p [m^2 kg^{-1}] is the specific particle surface area, l_0 [m] the initial particle size, M^p [kg] the particle mass, V^R [m^3] the working volume of the reactor, ϕ_{MS} the fraction of chalcopyrite in the particles, $I(\theta)$ the internal RTD and N^T is an estimation of the total number of particles in the reactor.

In a well-functioning heap, microbial ferrous iron oxidation kinetics are assumed to contribute significantly to the changing ferrous and ferric iron concentrations in the heap. The overall microbial ferrous iron oxidation rate, r_{bio} [mol Fe^{2+} m^{-3} h^{-1}], was determined from the ratio of total ferric to total ferrous iron concentration estimated using Eqs. 6 and 7. This approach was used as it has been recognised that the ferric and ferrous iron concentrations in the PLS is not representative of that at the ore surface and experimental data are not available. The specific microbial ferrous iron oxidation rate, $q_{Fe^{2+}}$ [mol Fe^{2+} mol C^{-1} h^{-1}], was determined as a function of the total microbial population within all phases in the heap, $C_{x,total}$ [mol C m^{-3}]. The Michaelis-Menten type rate expression (Eq. 10) as proposed by Hansford (1997) was used to describe the specific microbial ferrous iron oxidation rate, $q_{Fe^{2+}}$, as a function of the ferric to ferrous iron ratio.

$$q_{Fe^{2+}} = \frac{-r_{bio}}{C_{x,total}} = \frac{q^{max}_{Fe^{2+}}}{1 + K_s \cdot \left(\frac{C_{Fe^{3+}}}{C_{Fe^{2+}}}\right)} \quad (10)$$

where $q^{max}_{Fe^{2+}}$ [mol Fe^{2+} mol C^{-1} h^{-1}] is the maximum specific microbial ferrous iron utilisation rate and K_s is the dimensionless form of the Michaelis-Menten rate constant. Although *At. ferrooxidans* is able to oxidise both ferrous iron and reduced sulphur species, ferrous iron was assumed to be the preferred substrate during the exponential phase of microbial growth, as recently demonstrated by Moinier et al. (2013). For the purposes of the current study, the assumption that ferrous iron was the preferred substrate was validated using copper extraction data from the base case experiments (Govender et al., 2014).

Specific microbial growth rates were assumed to be governed by ferrous iron availability, hence, the specific microbial ferrous iron oxidation rate, with the yield coefficient, Y_{sx}, serving as the proportionality constant. This was based on the assumption of negligible microbial culture maintenance requirements. Specific microbial growth rates were determined from calibrated parameters for yield coefficients and microbial ferrous iron oxidation rates, using Eq. 11.

$$\mu_{x,i} = Y_{sx,i} \cdot \frac{r_{bio}}{C_{x,i}} = Y_{sx,i} \cdot q_{Fe^{2+}} \quad (11)$$

where *i* represents the different locations for microbial growth, i.e. total, PLS and ore-associated phases. The yield coefficient for substrate utilisation by the total microbial population within the mini-column reactor, $Y_{sx,total}$, was determined empirically from base case experimental data to be 0.05 mol $C_{x,total}$ (mol Fe^{2+})$^{-1}$. The yield coefficients for substrate utilisation by the microbial population in the PLS, $Y_{sx,PLS}$ [mol $C_{x,PLS}$ (mol Fe^{2+})$^{-1}$], and ore-associated phases, $Y_{sx,ore}$ [mol $C_{x,ore}$ (mol Fe^{2+})$^{-1}$], were estimated from the model fit and used to calculate maximum specific microbial growth rates, $\mu_{x,i}^{max}$ [h^{-1}], in each phase.

The model predictions for iron speciation in the ore-associated phases also inform the extent of microbial substrate utilisation and the magnitude of the yield coefficients in the different phases. In the absence of this supporting data, the model was developed using the assumption that the microbial substrate utilisation rate, r_{bio}, was representative of that within all phases in the heap, with separate yield coefficients used to distinguish the subsequent effect on microbial abundance in the bulk flowing PLS and ore-associated phases.

Advection-dispersion phenomena that incorporate microbial growth was applied to predict both temporal and spatial changes in microbial concentration within all boundaries within the agglomerate-scale heap, as in Eq. 12.

$$\frac{\partial C_{x,total}}{\partial t} = \mu_{x,total} \cdot C_{x,total} + D_Z \cdot \frac{\partial^2 C_{x,total}}{\partial z^2} - v \cdot \frac{\partial C_{x,total}}{\partial z} \quad (12)$$

where $C_{x,total}$ [mol C L^{-1}] is the microbial concentration in the total reactor volume (V^R) and $\mu_{x,total}$ [h^{-1}] is the specific microbial growth rate of the total population within the mini-column reactor.

Building on the biomass transport model presented previously by Govender et al. (2014), the hydrodynamic model was developed assuming that the microbial concentration gradient between the phases is the driving force for microbial transport across the phase boundary. In the proposed mathematical model, changes to the microbial abundance in the bulk flowing PLS, $C_{x,PLS}$ [mol C L^{-1}], were described as a function of microbial growth in the PLS, microbial transport through the ore bed facilitated by bulk solution flow dynamics as well as microbial transport across the interface between the bulk flowing PLS and ore-associated phases (Eq. 13).

$$\frac{\partial C_{x,PLS}}{\partial t} = \mu_{x,PLS} \cdot C_{x,PLS} + D_Z \cdot \frac{\partial^2 C_{x,PLS}}{\partial z^2} - v \cdot \frac{\partial C_{x,PLS}}{\partial z} - k_{att} \cdot (C_{x,PLS} - C_{x,ore}) + k_{det} \cdot (C_{x,ore} - C_{x,PLS}) \quad (13)$$

Microbial transport from the bulk flowing PLS to the ore-associated phases is described using the attachment term, k_{att} [h^{-1}], whilst microbial transport from the ore-associated phases to the bulk flowing PLS is described using the detachment term, k_{det} [h^{-1}]. Eq. 13 may be simplified mathematically by replacing the k_{det} and k_{att} terms with a net rate of transport term, k_{net}, and a single concentration difference term. However, individual microbial transport terms may provide insight into the difference in magnitude of microbial transport rates between the phases.

Further changes in microbial abundance in the ore-associated phases, $C_{x,ore}$ [mol C L^{-1}], are similarly modelled as a function of microbial growth and microbial transport across the stagnant solution associated with the mineral and void space, as shown in Eq. 14. Once again, the source terms relating to microbial attachment and detachment can be reduced to a net rate of microbial transport, k_{net}, across the concentration gradient. For demonstration purposes, these terms are decoupled here in an effort to describe microbial transport across the phase boundaries.

$$\frac{\partial C_{x,ore}}{\partial t} = \mu_{x,ore} \cdot C_{x,ore} + k_{att} \cdot (C_{x,PLS} - C_{x,ore}) - k_{det} \cdot (C_{x,ore} - C_{x,PLS}) \quad (14)$$

Although microbial transport along the height of the ore bed and out of the mini-column reactor was assumed to be induced by both the convective forces of the bulk flowing solution and the difference in microbial concentration between the phases, microbial transport to and from the ore-associated phases was assumed to be a result of a microbial concentration gradient only. It is proposed that the microbial concentration gradient was produced in response to the substrate concentration gradient; assuming a higher microbial production and simultaneous oxidation of ferrous iron in the ore-associated phases as compared to the bulk flowing PLS. *At. ferrooxidans* transport is facilitated *via* pili with "twitching motility" (Li et al., 2010) which may be triggered by cell to cell communication or quorum sensing in response towards a preferred environment with higher substrate availability, growth and maintenance requirements (Farah et al., 2005, Jerez, 2008, Soulère et al., 2008, Valenzuela et al., 2007).

Microbial transport in non-reactive porous soil systems has been modelled previously using the advection-dispersion equation (Tan et al., 1994, Taylor and Jaffé, 1990). The current model extends this approach by incorporating microbial growth kinetics as a function of the kinetics of microbial

substrate utilisation which, in turn, is limited by the rate of mineral dissolution, together with microbial attachment and detachment kinetics. The resulting estimation of *true* maximum specific growth rate (using Eq. 11) for the total microbial population within the agglomerate-scale heap was then applied to Eq. 15. As such, the theoretical ferric to ferrous iron ratio required to sustain the predicted microbial growth and abundance in the PLS and ore-associated phases can be estimated.

$$\mu_{x,total} \cdot C_{x,total} \cdot V^R = \mu_{x,PLS} \cdot C_{x,PLS} \cdot V_{PLS} + \mu_{x,ore} \cdot C_{x,ore} \cdot V_{ore} \quad (15)$$

The estimated volume of solution in the PLS, V_{PLS}, is 11.7 mL and that within the ore-associated phase, V_{ore}, is 2.3 mL, with a total reactor volume, V^R, of 14.0 mL (Govender et al., 2015b).

3.1. Application of the hydrodynamic transport model

3.1.1. Microbial growth and transport rates

For the purposes of comparison, simplifying assumptions were used to convert the microbial concentrations in the PLS and ore-associated phases from cfu per millilitre [cfu mL^{-1}] and cells per gram dry ore [cfu g DO^{-1}] to mol carbon per litre [mol C L^{-1}] using the known reactor working volume and total mass of dry ore within the mini-column reactor. The cell to mole carbon conversion was assumed to be 4.8 x 10^{-15} mol C $cell^{-1}$, based on a dry mass of 1.18 x 10^{-13} g $cell^{-1}$ (Moon, 1995) which compares well with the value of 1.59 x 10^{-13} g $cell^{-1}$ reported by Blight and Ralph (2008).

The mineral leaching rate constant (k_m), maximum specific ferrous iron utilisation rate ($q_{Fe^{2+}}^{max}$), Michaelis-Menten rate constant (K_m), overall yield coefficient ($Y_{sx,\,total}$), initial particle size distribution ($f_0(l_0)$), dispersion coefficient (D_z) and advection mass transfer rate (v) were estimated from data set Test A. Model fitting was performed using least squares regression analysis to estimate microbial yield coefficients in the PLS and ore-associated phases ($Y_{sx,PLS}$, $Y_{sx,ore}$) as well as microbial attachment (k_{att}) and detachment (k_{det}) rates. The data set from the repeated experiment Test B, and combined Test A and B data set, were then used to validate the model. The kinetic parameters used in the model are presented in Table 1.

Table 1: Summary of kinetic parameter values required for input into the hydrodynamic dispersion model as determined from base case experimental data

Kinetic parameter	Units	Empirical value
Mineral leaching rate constant, k_m	mol m^{-2} h^{-1}	1 x 10^{-6}
Maximum specific ferrous iron utilisation rate, $q_{Fe^{2+}}^{max}$	mol Fe^{2+} mol C^{-1} h^{-1}	1.61
Michaelis-Menten rate constant, K_m	Dimensionless	0.0025
Overall yield coefficient for substrate utilisation, $Y_{sx,\ total}$	mol C (mol Fe^{2+})$^{-1}$	0.05
Dispersion coefficient, D_z	m^2 h^{-1}	4.24 x 10^{-5}
Advection mass transfer rate, v	m h^{-1}	2.46 x 10^{-3}

Note: Particle size distribution data was presented previously in Govender et al. (2013).

The maximum specific ferrous iron utilisation rate, $q_{Fe^{2+}}^{max}$, and the dimensionless Michaelis-Menten rate constant, K_m, were determined from experimental data and have been presented previously as an outcome of the biomass model (Govender et al., 2014). The $q_{Fe^{2+}}^{max}$ value of 1.61 mol Fe^{2+} mol C^{-1} h^{-1} presented in this study, was lower than that of 8.8 mol Fe^{2+} mol C^{-1} h^{-1}, typically found for *At. ferrooxidans* in bioleaching systems (Boon, 1996, Breed and Hansford, 1999, Hansford, 1997). This result was expected since the cited studies were performed in continuous, well-mixed systems with fully suspended, milled sulphide mineral particles, whilst this study was conducted on crushed low-grade ore in the absence of supplementary ferrous iron in the feed, with pyrite occlusion in the low-grade ore further limiting substrate availability.

The total, PLS and ore-associated *apparent* maximum specific microbial growth rates were presented previously in Govender et al. (2013). These growth rates are defined as *apparent* rates since the effect of microbial transport between the phases was not taken into account in the calculation for specific growth rates in each phase. This assumption resulted in exaggerated growth rates in the PLS and under-estimated growth rates in the ore-associated phases. The current model aims to estimate these microbial transport rates and present *true* maximum specific microbial growth rates on whole ore.

The model predictions for PLS and ore-associated microbial concentration profiles are compared to those determined empirically, in Figure 2. From the onset, the model simulated the microbial concentration profiles in both the PLS and ore-associated phases successfully; in particular, the exponential growth region in both phases, the constant growth period observed after *ca*. 250 h in the PLS (Figure 2*a*), and the continued but slow increase in microbial concentration in the ore-associated phase (Figure 2*b*).

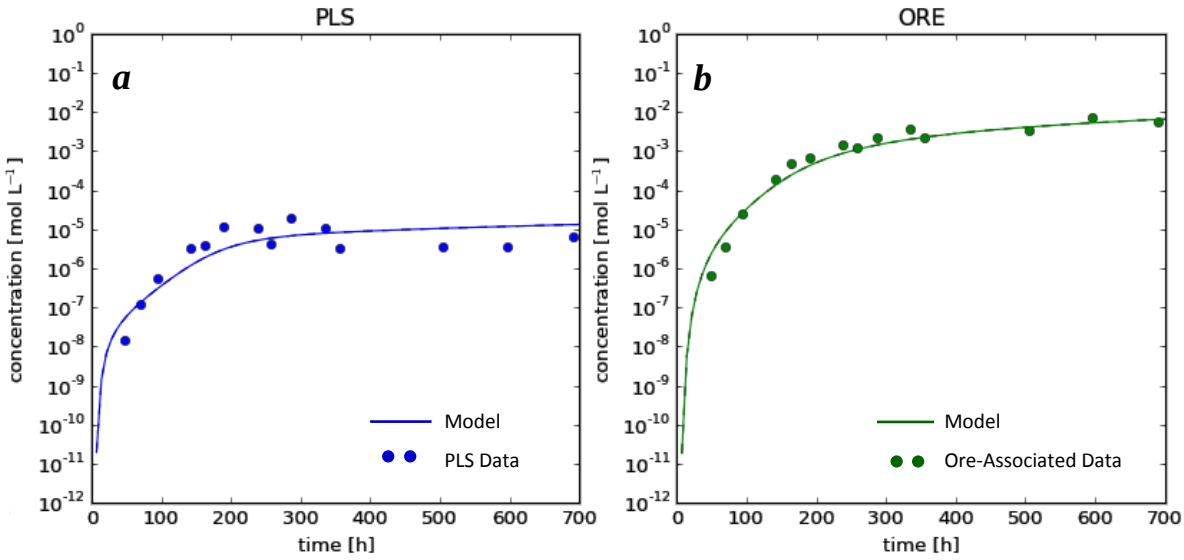

Figure 2: Model prediction of changes in microbial abundance in the (a) bulk flowing PLS and (b) ore-associated phases with time, using the combined base case experimental data set

A subset of the PLS microbial concentration data is presented in Figure 2*a*, with the complete data set presented previously in Govender et al. (2014) showing an initial dip in microbial abundance in the PLS, a result of initial and rapid microbial attachment. Although the model was able to predict low microbial concentrations over the first few hours of the experiment, it did not predict this period of initial and rapid attachment. This type of microbial behaviour, however, was predicted appropriately by the biomass transport model (Govender et al., 2014). The hydrodynamic dispersion model does predict the more rapid increase in the ore-associated population which may represent the initial period of attachment.

The model outputs for yield coefficients, $Y_{sx,PLS}$ and $Y_{sx,ore}$, are 0.00027 and 0.012 mol C (mol Fe^{2+})$^{-1}$ respectively. These yield coefficients correspond to *true* maximum specific growth rates in the PLS and ore-associated phases of 0.0004 and 0.019 h^{-1} respectively. The apparent maximum specific growth rates as determined from empirical data without accounting for microbial transport between the phases may be compared to the *true* maximum specific growth rates as predicted by the biomass and hydrodynamic models (Table 2).

The most notable difference in the hydrodynamic model output was the higher *true* maximum specific growth rates predicted for the ore-associated phase over the PLS (Table 2). This finding, together with the relatively low maximum specific growth rate in the PLS, suggests that microbial growth occurs primarily within the largely stagnant interstitial solution and mineral attached phases, with a proportion of the new cells being transported away from the mineral surface. The predicted *true* maximum specific growth rates in the ore-associated phase corresponded to a culture doubling time of 36.5 h. The predicted ore-associated growth rate and doubling time is comparable to literature values

for microbial growth on pulverised low-grade Kennecott ore at similar substrate-free test conditions (Plumb et al., 2008), where the specific growth rate is estimated from further analysis of data to be 0.028 h^{-1}, with a corresponding doubling time of 24.8 h.

Since microbial transport out of the ore bed through advection is incorporated into the equation describing the change in total microbial abundance within all phases in the heap (Eq. 12), the predicted total *true* maximum specific growth rate of 0.088 h^{-1}, with a doubling time of 7.9 h, was higher than that for the ore-associated phase of 0.019 h^{-1}, with a doubling time of 36.5 h. These doubling times (Table 2) are comparable to those reported previously for *At. ferrooxidans* growth on chalcopyrite mineral of 25 h (Plumb et al., 2008) and 13.9 h (McGoran et al., 1969), corresponding to specific growth rates of 0.028 and 0.050 h^{-1} respectively. The prediction for total *true* maximum specific growth rate from the current model compared more favourably to previously reported literature values, than that predicted by the biomass transport model (Govender et al. 2014).

Table 2: Maximum specific growth rates as determined from experimental data and predicted by the biomass (Govender et al., 2014) and hydrodynamic microbial transport models, using Michaelis-Menten type rate kinetics

		Test A & B combined	Biomass model	Hydrodynamic model
$\mu_{x,PLS}^{max}$	h^{-1}	0.741 ± 0.011	0.736	0.0004
$\mu_{x,ore}^{max}$	h^{-1}	0.054 ± 0.006	0.048	0.019
$\mu_{x,total}^{max}$	h^{-1}	0.733 ± 0.013	0.739	0.088

The predicted rate of microbial transport from the PLS to the ore-associated phases *via* microbial attachment (k_{att}) was estimated to be 1.2 x10^{-7} h^{-1}, whilst the rate of microbial transport from the ore-associated phases to the bulk flowing PLS *via* detachment (k_{dett}) was estimated to be 5 x10^{-5} h^{-1}. The higher rate of microbial transport from the ore-associated phases to the PLS, predicted by the hydrodynamic model, was in contrast to that previously predicted by the biomass model. The hydrodynamic model, therefore, supports the hypothesis that microbial growth is more prolific in the ore-associated phases with subsequent transport to the bulk flowing PLS.

The success of the current hydrodynamic model in predicting *true* maximum specific growth rates as a function of microbial transport may lie in the incorporation of attachment and detachment rates that are a function of the microbial concentration gradient, into the advection-dispersion model (Eqs. 13 and 14). While it is recognised that attachment and detachment are also impacted by physicochemical surface properties of the microorganisms and mineral, surface topology of the mineral and fluid flow conditions, these are not varied in this study to allow the impact of concentration driving force to be determined. Current understanding suggests that in the first few hours after inoculation, the rate of

517 microbial attachment is significantly higher than the rate of microbial detachment, with $k_{att}(C_{x,PLS} -$
518 $C_{x,ore}) >> k_{det}(C_{x,ore} - C_{x,PLS})$. Based on the attachment and detachment rates determined using the
519 model, it can be postulated that once steady state conditions are reached, the rate of microbial
520 detachment is much greater than microbial attachment, i.e. $k_{det}(C_{x,ore} - C_{x,PLS}) >> k_{att}(C_{x,PLS} - C_{x,ore})$,
521 owing to growth at the mineral surface. The low microbial transport rates as compared to growth rates
522 may require further study for refinement; in this study, the attachment and detachment rate constants
523 (k_{att} and k_{det}) were postulated to remain unchanged despite the slopes of the concentration-time curves
524 change over the region of exponential microbial growth and constant growth (Figure 2*a* and *b*). The
525 use of a single value for each transport rate constant over the short duration of the experiments was
526 sufficient in the current study to decouple the effect of microbial transport from microbial growth.
527
528 Using the hydrodynamic dispersion model, 3D plots were generated to demonstrate the change in
529 microbial concentration profiles in the PLS and ore-associated phases with time, as well as the change
530 in microbial distribution at t = 700 h with fractional distance from the top of the ore bed (top = 0.0).
531 The model predicted the rapid increase in PLS microbial concentration with time over the initial
532 period of *ca*. 250 h, followed by the period of slower increase (Figure 3*b*(i)). The microbial
533 distribution in the void PLS volume (Figure 3*a* (ii)) was observed to be *ca*. 10 times lower at the top
534 of the column than at the bottom, with the microbial abundance in the PLS increasing linearly with
535 the depth of the ore bed. This observation, however, may be subject to the hydrodynamic properties of
536 the bulk flowing solution which is largely influenced by both the height to diameter ratio of the ore
537 bed (Kappes, 2002) as well as flow rate of the irrigation solution (Pantelis and Ritchie, 1991, Pantelis
538 and Ritchie, 1992).
539
540 Microbial abundance in the ore-associated phases, shown in Figure 3*b*, was found to increase non-
541 linearly from the top to the bottom of the ore bed (Figure 3*b*(ii)), with a significantly higher microbial
542 abundance associated with the ore than that observed in the PLS. A high microbial concentration was
543 observed at the bottom of the ore bed by the end of the experiment. The observations suggest that for
544 this particular reactor configuration, the microbial population associated with the ore bed is not
545 uniformly distributed throughout the bed. This is consistent with the transfer of micro-organisms
546 through the bed, associated with fluid flow under gravity.
547

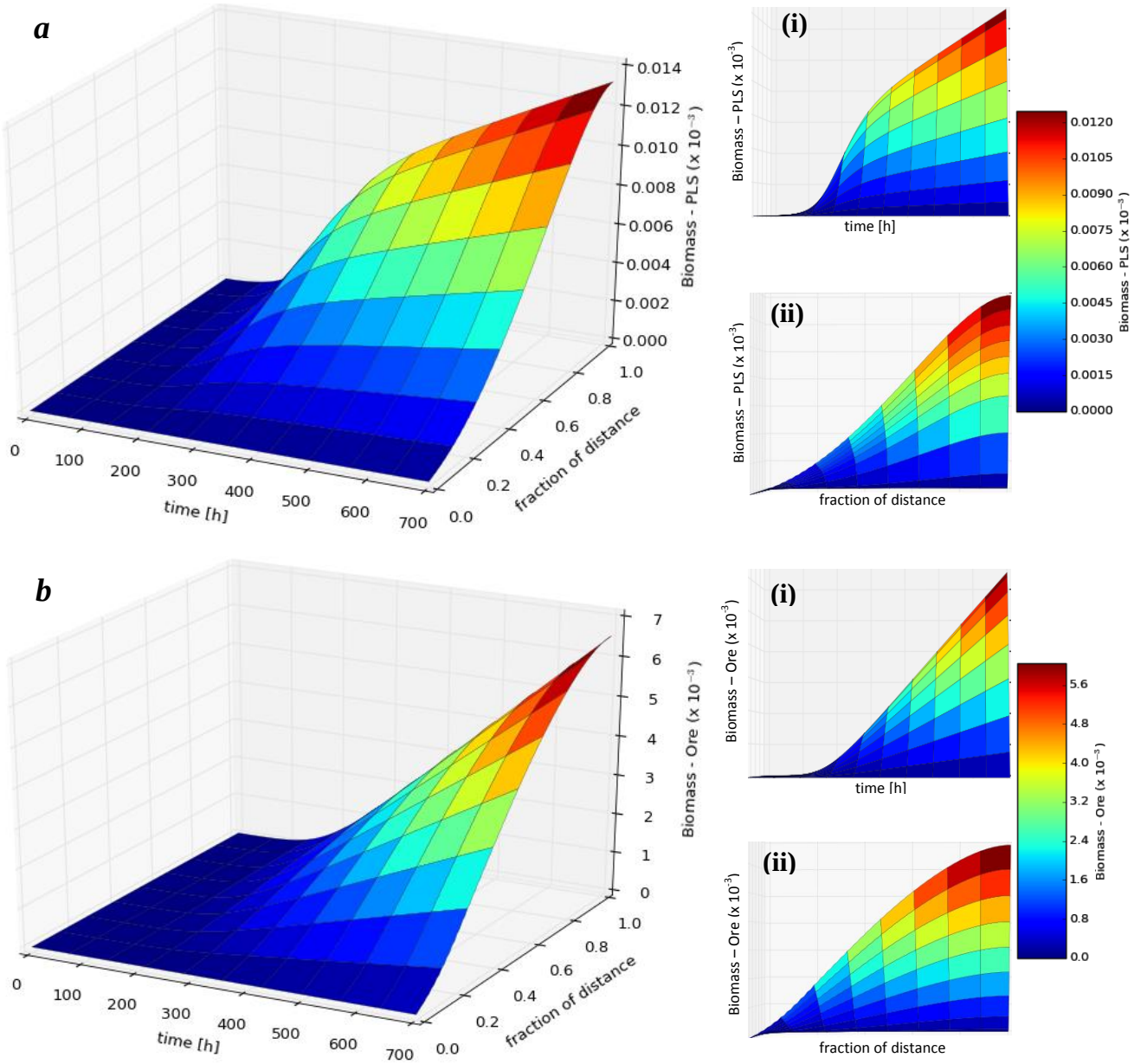

Figure 3: 3D Plot illustrating changes to microbial concentration in the (a) bulk flowing PLS and (b) ore-associated phases with time and fraction of distance along the ore bed (top = 0.0) at the termination of the experiment. Inserts (i) highlights the change in biomass concentration with time and inserts (ii) highlights the change in biomass concentration with the depth of the bed.

3.1.2. Ferric to ferrous iron concentrations within the ore bed

In an effort to decouple the concentrations of ferric and ferrous iron in the respective phases, model predictions of overall iron concentrations relative to those measured in the PLS, were compared (Figure 4). Using the combined data set, the ferric and ferrous iron concentrations measured in the bulk flowing PLS were used to estimate the mineral leach and microbial substrate utilisation kinetics for input into the model to describe the total microbial growth kinetics. The resulting model-predicted substrate utilisation kinetics in the PLS and ore-associated phases were then used to determine the ferrous and ferric iron concentrations required to sustain the combined PLS and ore-associated

561 microbial populations. The difference between the model prediction and the measured concentrations
562 was assumed to represent that in the ore-associated phases (Eq. 5).
563
564 The model prediction of higher overall ferric and ferrous iron concentrations than that measured in the
565 PLS supports the assumption of higher iron concentrations in the ore-associated phases. The predicted
566 overall iron concentrations follow similar trends to that shown by the measured data set. For example,
567 the model describes the expected initial production of ferrous iron (Figure 4*b*) as a result of
568 instantaneous oxidation of the mineral by ferric iron, depicted by the initial decrease in ferric iron
569 concentration (Figure 4*a*). The subsequent decrease in ferrous iron concentration in response to
570 increased microbial activity was also described by the model. In addition, the model predicts an
571 absence of residual ferrous iron concentration by *ca*. 200 h in the PLS and consequently, the ore-
572 associated phases.
573

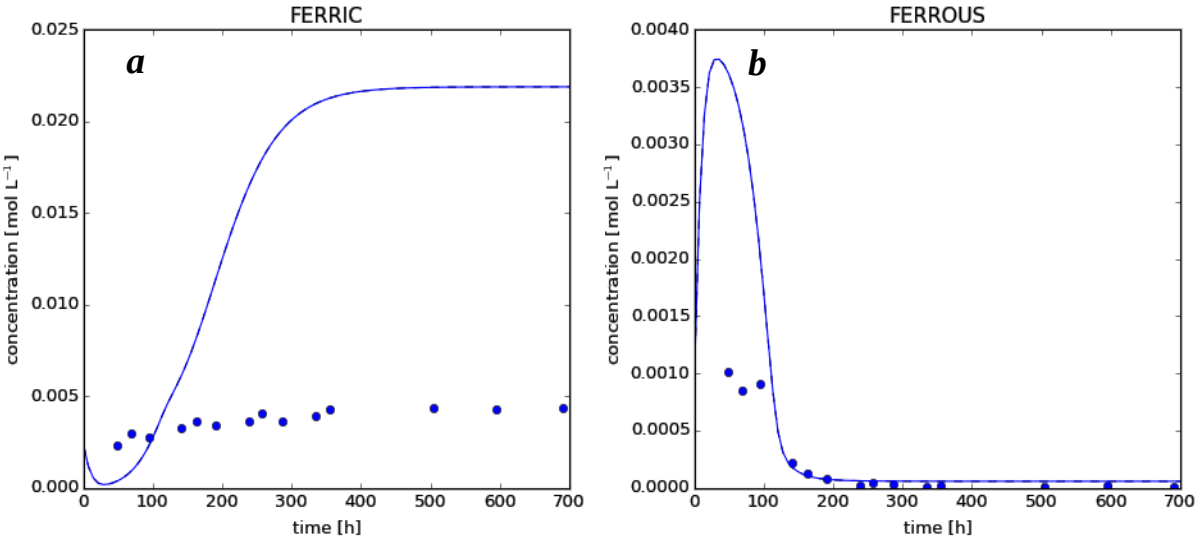

574
575
576 **Figure 4: Model predictions for overall (a) ferric and (b) ferrous iron concentrations (▬) in comparison**
577 **with ferric and ferrous iron concentrations measured in the bulk flowing PLS [●].**
578

579 ### 3.2. Model sensitivity analysis

580 The trends presented in Figure 3 and Figure 4 are subject to the current test conditions, more
581 specifically, the dispersion and advection properties of the bulk flowing solution. The dispersion
582 coefficient, D_Z, and advection mass transfer rate, v, were estimated from RTD experiments to be 4.24
583 x 10^{-5} m^2 h^{-1} and 2.46 x 10^{-3} m h^{-1}, respectively (Table 1). A sensitivity analysis was performed to
584 determine the effect of varying these parameters on the model outcomes (Figure 5). For this analysis,
585 the dispersion coefficient was doubled to 8.48 x 10^{-5} m^2 h^{-1} (Figure 5*a*) and halved to 2.12 x 10^{-5} m^2 h^{-1}
586 (Figure 5*b*). The advection mass transfer rate was varied through irrigation rates of 2 L m^{-2} h^{-1} to 2.5

587 L m^{-2} h^{-1} and 1 L m^{-2} h^{-1}, respectively. As such, the equivalent advection mass transfer rates were 3.07
588 x 10^{-3} m h^{-1} (Figure 5*c*) and 1.23 x 10^{-3} m h^{-1} (Figure 5*d*), respectively.
589
590 **3.2.1. Sensitivity of hydrodynamic model to variations in dispersion coefficient**
591 An increase in D_z resulted in an increase to the initial microbial concentrations found in the PLS and
592 ore-associated phases followed by a decrease in microbial abundance in both phases over the steady
593 state period, as illustrated in Figure 5*a*. Since increased dispersion increases the mixing or contacting
594 between the PLS and ore-associated phases, a larger portion of the inoculum is uniformly distributed
595 within the column initially, however, this will also facilitate increased transport of micro-organisms in
596 the bulk solution with depth of the ore bed. In addition, increased contacting would result in a higher
597 rate of attachment, k_{att}, with a larger population of micro-organisms in the PLS transporting to the ore-
598 associated phase. This would be observed by the decrease in the difference between the ore-associated
599 microbial abundance as predicted by the model and that of the model response to an increase in the
600 dispersion coefficient. Decreasing the dispersion coefficient (Figure 5*b*), decreased the retention of
601 inoculum in the mini-column reactor as a result of less contacting between the phases and possible
602 poor mixing or channelling of solution within the ore bed. Preferential flow within the ore bed would
603 result in greater detachment of the ore-associated population into the bulk PLS and out of the ore bed.
604
605 **3.2.2. Sensitivity of hydrodynamic model to variations in advection mass transfer coefficient**
606 The advection mass transfer coefficient (*v*) was varied by increasing the feed irrigation rate from 2 L
607 m^{-2} h^{-1} to 2.5 L m^{-2} h^{-1} (Figure 5*c*) and decreasing the irrigation rate to 1 L m^{-2} h^{-1} (Figure 5*d*). Beyond
608 these constraints, the model predictions for microbial concentration along the height of the ore bed
609 became unstable, yielding erratic concentration profiles. The variations resulted in significant changes
610 to the predicted microbial concentrations in the PLS and the ore-associated phases. A decrease in the
611 retention of inoculum within the mini-column with increasing *v* was predicted, resulting in decreased
612 microbial abundance in the PLS and ore-associated phases (Figure 5*c*). By decreasing *v*, a greater
613 population of micro-organisms was predicted to remain within the ore bed, resulting in an increase in
614 microbial abundance in the PLS and ore-associated phases (Figure 5*d*). The effect of varying
615 irrigation rates on inoculum retention and microbial colonisation was supported by the corresponding
616 change in the rate of ferrous iron oxidation at higher irrigations (results not shown).

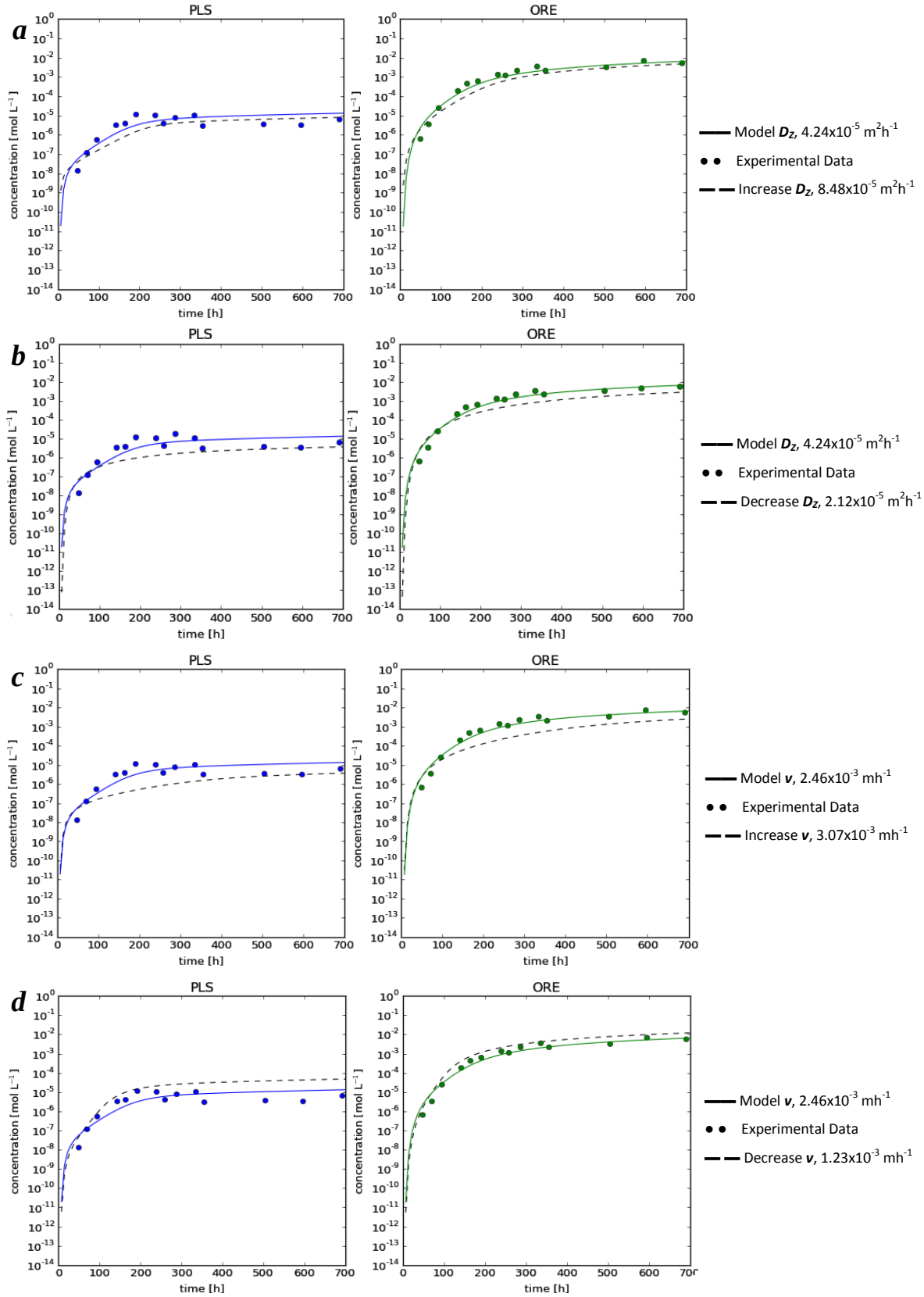

Figure 5: Sensitivity of proposed model to changes in dispersion coefficient (D_Z) and advective transfer rate (v), with (a) increasing D_Z to 8.48 x 10^{-5} m^{2}h^{-1}, (b) decreasing D_Z to 2.12 x 10^{-5} m^{2}h^{-1}, (c) increasing v to 3.07 x 10^{-3} mh^{-1} and (d) decreasing v to 1.23 x 10^{-3} mh^{-1}. The fitted model is represented by the solid line and the model predicted outcome following a change in parameter by the dashed line.

3.2.3. Sensitivity of hydrodynamic model to variations in inoculum size

The sensitivity analysis on the hydrodynamic model was extended to include the response of the model to variations in an operating condition, in particular, to an increase and decrease in inoculum concentration. The effect of varying inoculum size on microbial growth and activity using the current experimental system has been discussed previously in Govender et al. (2015a); however, direct comparison of the model predictions with experimental data cannot be made since the *At. ferrooxidans* pre-culturing conditions and feed composition vary.

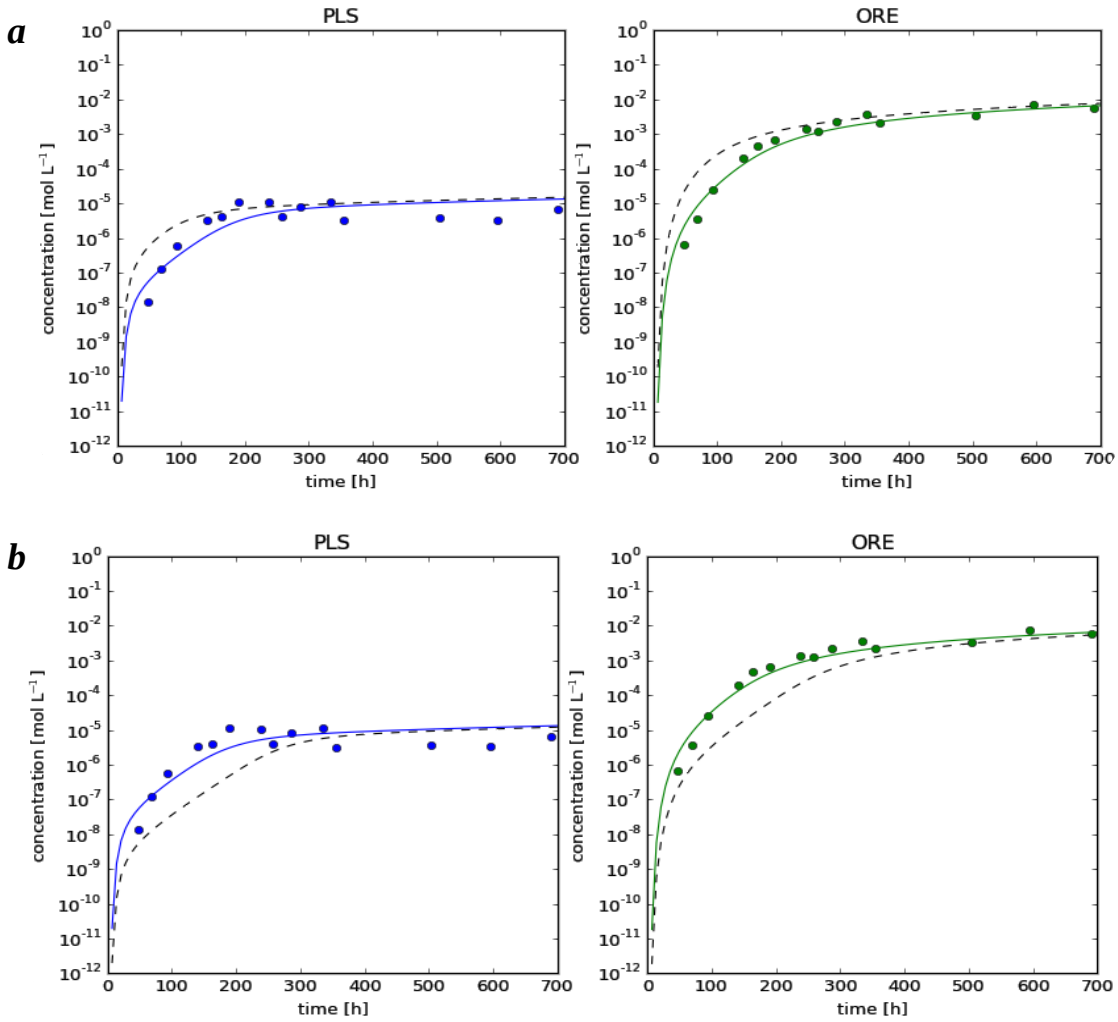

Figure 6: Sensitivity of the proposed model predictions of the change in microbial concentrations in the PLS and ore-associated phases, to (a) a ten-fold increase in inoculum concentration and (b) a ten-fold decrease in inoculum concentration. The fitted model is represented by the solid line [—], experimental data by shaded circles [●] and the model predicted outcome following a change in parameter by the dashed line [- - - -].

As observed from Figure 6*a*, an increase in inoculum size increased the initial microbial abundance in each of the phases. An increase in inoculum size has been shown to produce a more rapid increase in microbial number, which is in agreement with that observed in previous studies (Govender et al., 2015a, Tupikina et al., 2014). This effect was not observed since the hydrodynamic model exhibits

poor resolution over this initial period. As previously mentioned, the model also did not simulate the initial decrease in PLS concentration as a result of rapid microbial attachment to the mineral (Figure 2*a*). Initial microbial populations reporting to the PLS and ore-associated phases were observed to decrease with a decrease in inoculum size (Figure 6*b*) and the time required before microbial numbers increase substantially was expected to increase.

However, irrespective of inoculum size, the final maximum microbial concentrations in both the PLS and ore-associated phases remain unchanged. In addition, the model predicted that an increase in inoculum size results in the maximum microbial concentration being reached earlier than with a lower inoculum size. The abovementioned model responses to varying inoculum concentration were also observed in the empirical data presented previously (Govender et al., 2015a).

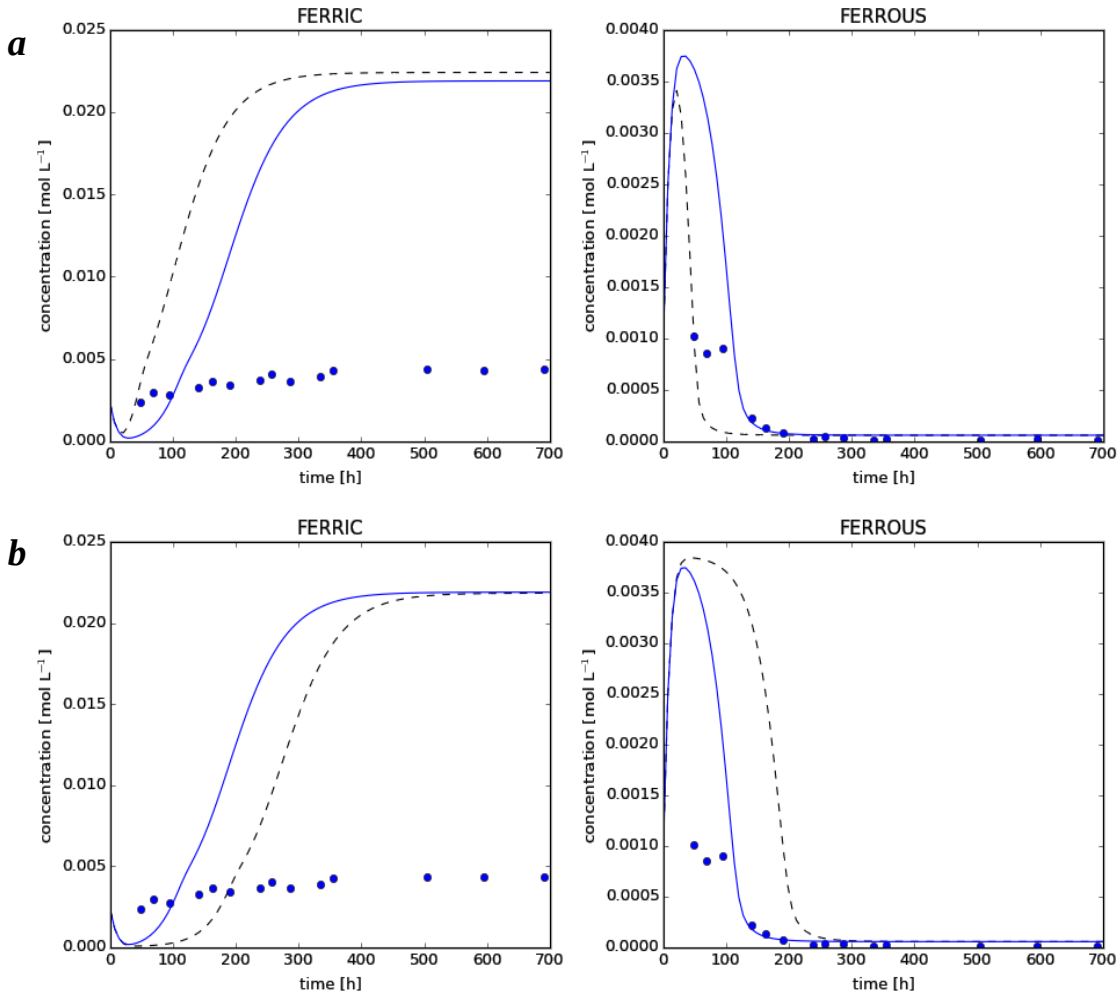

Figure 7: Sensitivity of the proposed model predictions of overall ferric and ferrous iron concentrations, to (a) a ten-fold increase in inoculum concentration and (b) a ten-fold decrease in inoculum concentration. The fitted model is represented by the solid line [—], experimental data by shaded circles [●] and the model predicted outcome following a change in parameter by the dashed line [- - - -].

An increase in inoculum size resulted in a more rapid increase in microbial activity, as observed in the predicted overall ferric and ferrous iron concentrations (Figure 7*a*). The ten-fold increase in inoculum size produced an approximate decrease the time for onset of microbial activity of 50 h. Similarly, a ten-fold decrease in inoculum size resulted in a predicted increase in time delay for onset of microbial activity of *ca*. 100 h (Figure 7*b*).

4. Conclusions

Recent mineral bioleaching studies have demonstrated the significant difference between the microbial populations in the PLS and ore-associated phases. This has impact on the interpretation of the data obtained during monitoring of heap bioleaching systems. However, no studies have yet developed and validated an appropriate mathematical model to decouple the effects of microbial transport between these phases and microbial growth kinetics. The proposed hydrodynamic model was developed assuming that the microbial concentration gradient between the PLS and ore-associated phases was the driving force, together with substrate availability, for microbial attachment to and detachment from the ore-associated phases, with transport being facilitated by advection-dispersion properties of the bulk flowing solution. Mineral leach kinetics were assumed to be dependent on the ferric to ferrous iron ratio and modified to include the population balance model (PBM), thus providing a better estimation of the contribution of surface-based reactions to the overall mineral leach rate. Microbial substrate utilisation kinetics were described assuming a Michaelis-Menten type relationship with ferric to ferrous iron ratio and related to growth kinetics through the yield coefficient.

This proposed model successfully predicted the changes in microbial concentration in the PLS and ore-associated phases using an advection-dispersion equation, which incorporated terms for microbial growth, attachment and detachment rates. The model prediction for the *true* maximum specific growth rate in the ore-associated phases was found to be significantly greater than that predicted in the PLS. This result is in accordance with the hypothesis that within a whole ore bioleaching system, microbial growth and activity occurs primarily in the ore-associated phases, where ferrous iron availability is enhanced. Hence, the microbial abundance in the PLS was a result of microbial transport from the ore-associated phases to the PLS. This hydrodynamic dispersion model provides insight into true estimates for microbial growth rates within heap bioleaching systems. With further refinement and validation, the model, therefore, offers the potential for the estimation of the relative microbial abundance in the ore-associated phases, given the microbial concentration and activity measured in the PLS, and without the need to sample the heap for analysis the ore.

Since the model is based on the hydrodynamic properties of the bulk solution, the effect of variables such as solution flow rate, bulk density and reactor configuration on the model outputs require further

694 study for refinement of these parameters for enhanced model predictions. These variables are
695 particularly important for the estimation of dispersion coefficients and the advection transfer rates,
696 which have a significant effect on the model outputs. In addition, the model may be improved through
697 the inclusion of ferric and ferrous iron concentrations measured at the mineral interface, which will
698 allow for further validation the model.
699

700 ## 5. List of symbols

$\mu_{x,pls}$	Specific microbial growth rate in the PLS	h^{-1}
$\mu_{x,ore}$	Specific microbial growth rate in the ore-associated phase	h^{-1}
$\mu_{x,total}$	Specific microbial growth rate in the total population	h^{-1}
$\mu_{x,i}^{max}$	Maximum microbial specific growth rate for each phase	h^{-1}
ϕ_{MS}	Fraction of pure mineral sulphide in ore	dimensionless
τ	Mean residence time	h
θ	Age of particle	h
A^P	Particle specific surface area	$m^2\ kg^{-1}$
C_{Fe}^{2+}	Ferrous iron concentration	$molFe^{2+}\ L^{-1}$
C_{Fe}^{3+}	Ferric iron concentration	$molFe^{3+}\ L^{-1}$
$C_{x,pls}$	Microbial concentration in the PLS	$molC\ L^{-1}$
$C_{x,ore}$	Microbial concentration in the ore-associated phase	$molC\ L^{-1}$
$C_{x,total}$	Microbial concentration in the total population	$molC\ L^{-1}$
D_r	Dispersion coefficient in radial direction	$m^2\ h^{-1}$
D_z	Dispersion coefficient	$m^2\ h^{-1}$
$f_0\ (l_0)$	The normal distribution representing the probability of particles in a specific size range	m^{-1}
$I\ (\theta)$	The internal age distribution of particles	h^{-1}
k_{att}	Microbial attachment rate constant	h^{-1}
k_{det}	Microbial detachment rate constant	$mol\ m^{-2}\ h^{-1}$
k_m	Mineral leach rate constant	$mol\ m^{-2}\ h^{-1}$
K_s	Michaelis-Menten constant for substrate utilisation	dimensionless
l_0	Initial particle size or diameter	m
M^P	Mass of a particle	kg
n	Order of mineral leach reaction	dimensionless
N^T	Total number of particles in the reactor	dimensionless
q_{Fe}^{2+}	Microbial specific ferrous iron oxidation rate	$molFe^{2+}\ molC\ h^{-1}$
q_{Fe2+}^{max}	Maximum microbial specific ferrous iron oxidation rate	$molFe^{2+}\ molC\ h^{-1}$

r_{bio}	Rate of microbial ferrous iron oxidation	$molFe^{2+}\ L^{-1}\ h^{-1}$
r''_{min}	Intrinsic mineral surface reaction rate	$mol\ m^{-2}\ h^{-1}$
r^R	Overall mineral leach rate	$mol\ m^{-3}\ h^{-1}$
t	Time	h
v	Advection mass transfer coefficient	$m\ h^{-1}$
V^R	Total working liquid volume in reactor	m^3 or L
V_{PLS}	Volume of bulk flowing solution or PLS within ore bed	L
V_{ore}	Volume of stagnant interstitial solution within ore bed	L
$Y_{sx,pls}$	Microbial yield coefficient in PLS	$molC_{x,PLS}\ [molFe^{2+}]^{-1}$
$Y_{sx,ore}$	Microbial yield coefficient in ore=associated phase	$molC_{x,ore}\ [molFe^{2+}]^{-1}$
$Y_{sx,total}$	Microbial yield coefficient in all phase in ore bed	$molC_{x,total}\ [molFe^{2+}]^{-1}$
z	Depth of bed	m

6. Acknowledgements

The financial assistance of the Department of Science and Technology (DST) and the National Research Foundation (NRF) of South Africa, through the South African Research Chairs Initiative (SARChI UID64778) is hereby acknowledged. Opinions expressed and conclusions arrived, are those of the author and are not necessarily to be attributed to the NRF.

7. References

Batty, J. D. & Rorke, G. V. 2006. Development and commercial demonstration of the BioCOP thermophile process. *Hydrometallurgy,* 83**,** 83-89.

Bhappu, R. B., Johnson, P. H., Brierley, J. A. & Reynolds, D. H. 1969. Theoretical and practical studies on dump leaching. *AIME Transactions,* 244**,** 307-320.

Blight K.R. and Ralph D.E. 2008. Maximum yield and standard enthalpy of growth of iron-oxidising bacteria. *Hydrometallurgy* 93, 66-71.

Boon, M. 1996. *Theoretical and experimental methods in the modelling of the bio-oxidation kinetics of sulphide minerals.* PhD PhD, Delft University of Technology.

Bouffard, S. C. 2005. Review of agglomeration practice and fundamentals in heap leaching. *Mineral Processing and Extractive Metallurgy Review,* 26**,** 233-294.

Bouffard, S. C. & West-Sells, P. G. 2009. Hydrodynamic behaviour of heap leach piles: Influence of testing scale and material properties. *Hydrometallurgy,* 98**,** 136-142.

Breed, A. W. & Hansford, G. S. 1999. Modeling continuous bioleach reactors. *Biotechnology and Bioengineering,* 64**,** 671-677.

Chen, B.-W. & Wen, J.-K. 2013. Feasibility study on heap bioleaching of chalcopyrite. *Rare Metals,* 32**,** 524-531.

725 Chiume, R. A., Minnaar, S. H., Ngoma, I. E., Bryan, C. G. & Harrison, S. T. L. 2012. Microbial
726 colonisation in heaps for mineral bioleaching and the influence of irrigation rate. *Minerals*
727 *Engineering*, 39**,** 156-164.
728 Córdoba, E. M., Muñoz, J. A., Blázquez, M. L., González, F. & Ballester, A. 2008. Leaching of
729 chalcopyrite with ferric ion. Part II: Effect of redox potential. *Hydrometallurgy*, 93**,** 88-96.
730 Dew, D. W., Rautenbach, G. F., van Hille, R. P., Davis-Belmar, C. S., Harvey, I. J. & Truelove, J. S.
731 2011. High temperature heap leaching of chalcopyrite: Method of evaluation and process model
732 evaluation. *Percolation Leaching: The status globally and in Southern Africa 2011*. Johannesburg,
733 South Africa: The Southern African Institute of Mining and Metallurgy.
734 Dixon, D. G. 2000. Analysis of heat conservation during copper sulphide heap leaching.
735 *Hydrometallurgy*, 58**,** 27-41.
736 Escobar, B., Jedlicki, E., Wiertz, J. & Vargas, T. 1996. A method for evaluating the proportion of free
737 and attached bacteria in the bioleaching of chalcopyrite with *Thiobacillus ferrooxidans*.
738 *Hydrometallurgy*, 40**,** 1-10.
739 Fagan-Endres M.A., Harrison S.T.L., Johns M.L., and Sederman A.J. 2015. Magnetic resonance
740 imaging characterisation of the influence of flowrate on liquid distribution in drip irrigated heap
741 leaching. *Hydrometallurgy* 158, 157-164.
742 Farah, C., Vera, M., Morin, D., Haras, D., Jerez, C. A. & Guiliani, N. 2005. Evidence for a functional
743 quorum-sensing type AI-1 system in the extremophilic bacterium *Acidithiobacillus ferrooxidans*.
744 *Applied and Environmental Microbiology*, 71**,** 7033-7040.
745 Gehrke, T., Telegdi, J., Thierry, D. & Sand, W. 1998. Importance of extracellular polymeric
746 substances from *Thiobacillus ferrooxidans* for bioleaching. *Applied and Environmental*
747 *Microbiology*, 64**,** 2743-2747.
748 Govender, E., Bryan, C. G. & Harrison, S. T. L. 2013. Quantification of growth and colonisation of
749 low grade sulphidic ores by acidophilic chemoautotrophs using a novel experimental system.
750 *Minerals Engineering*, 48**,** 108-115.
751 Govender, E., Bryan, C. G. & Harrison, S. T. L. 2015a. Effect of physico-chemical and operating
752 conditions on the growth and activity of *Acidithiobacillus ferrooxidans* in a simulated heap
753 bioleaching environment. *Minerals Engineering*, 75**,** 14-25.
754 Govender, E., Bryan, C. G. & Harrison, S. T. L. 2015b. A novel experimental system for the study of
755 microbial ecology and mineral leaching within a simulated agglomerate-scale heap bioleaching
756 system. *Biochemical Engineering Journal*, 95**,** 86-97.
757 Govender, E., Kotsiopoulos, A., Bryan, C. G. & Harrison, S. T. L. 2014. Modelling microbial
758 transport in simulated low-grade heap bioleaching systems: The biomass transport model.
759 *Hydrometallurgy*, 150**,** 299-307.

760 Govender-Opitz, E., Kotsiopoulos, A., Bryan, C. G. & Harrison, S. T. L. 2016. Insight into solute and
761 microbial transport in heap (bio)leaching systems using residence time distribution.
762 *Hydrometallurgy,* in press.
763 Hansford, G. S. 1997. Recent developments in modeling the kinetics of bioleaching. *In:* Rawlings, D.
764 E. (ed.) *Biomining: Theory, Microbes and Industrial Processes.* 1st ed. Berlin, Germany: Springer-
765 Verlag.
766 Hansford, G. S. & Vargas, T. 2001. Chemical and electrochemical basis of bioleaching processes.
767 *Hydrometallurgy,* 59**,** 135-145.
768 Hiroyoshi, N., Kitagawa, H. & Tsunekawa, M. 2008. Effect of solution composition on the optimum
769 redox potential for chalcopyrite leaching in sulfuric acid solutions. *Hydrometallurgy,* 91**,** 144-149.
770 Ilankoon, I. M. S. K., Cole, K. E. & Neethling, S. J. 2013. Measuring hydrodynamic dispersion
771 coefficients in unsaturated packed beds: Comparison of PEPT with conventional tracer tests.
772 *Chemical Engineering Science,* 89**,** 152-157.
773 Ilankoon I.M.S.K and Neethling S.J. 2014. Transient liquid holdup and drainage variations in gravity
774 dominated non-porous and porous packed beds. *Chemical Engineering Science* 116, 398-405.
775 Jerez, C. A. 2008. The use of genomics, proteomics and other OMICS technologies for the global
776 understanding of biomining microorganisms. *Hydrometallurgy,* 94**,** 162-169.
777 Johnson, D. B. 1995. Selective solid media for isolating and enumerating acidophilic bacteria. *Journal*
778 *of Microbiological Methods,* 23**,** 205-218.
779 Johnson, D. B., Joulian, C., d'Hugues, P. & Hallberg, K. B. 2008. *Sulfobacillus benefaciens* sp. nov.,
780 an acidophilic facultative anaerobic *Firmicute* isolated from mineral bioleaching operations.
781 *Extremophiles,* 12**,** 789-798.
782 Kappes, D. W. 2002. Precious metal heap leach design and practice. Reno, Nevada: Kappes, Cassiday
783 & Associates.
784 Kinzler, K., Gehrke, T., Telegdi, J. & Sand, W. 2003. Bioleaching - a result of interfacial processes
785 caused by extracellular polymeric substances (EPS). *Hydrometallurgy,* 71**,** 83-88.
786 Kotsiopoulos, A., Hansford, G. S. & Rawatlal, R. 2008. An approach of segregation in modeling
787 continuous flow tank bioleach systems. *AIChE Journal,* 54**,** 1592-1599.
788 Kotsiopoulos, A., Hansford, G. S. & Rawatlal, R. 2012. A dynamic analysis of chalcopyrite
789 bioleaching in continuous flow reactor systems. *AIChE Journal,* 58**,** 2429-2440.
790 Leahy, M. J., Davidson, M. R. & Schwarz, M. P. A column bioleaching model for chalcocite: An
791 investigation of oxygen limitation and bacterial inoculation on leaching. *In:* Spry, A., Burt, K. &
792 Stiffe, J., eds. Bac-Min, 2004 Melbourne, Australia. Aus.I.M.M, 41-47.
793 Li, Y.-Q., Wan, D.-S., Huang, S.-S., Leng, F.-F., Yan, L., Ni, Y.-Q. & Li, H.-Y. 2010. Type IV pili of
794 *Acidithiobacillus ferrooxidans* are necessary for sliding, twitching motility, and adherence.
795 *Current Microbiology,* 60**,** 17-24.

Lizama, H. M. 2001. Copper bioleaching behaviour in an aerated heap. *International Journal of Mineral Processing,* 62**,** 257-269.

Marshall, K. C. 1976. *Interfaces in microbial ecology,* Cambridge, Massachusetts, Harvard University Press.

McFarlane, A., Kuhar, L., Turner, N., Botsis, N. & Ravi, S. 2011. Defining the properties of good agglomerates. *Percolation Leaching: The status globally and in Southern Africa 2011.* Johannesburg, South Africa: The Southern African Institute of Mining and Metallurgy.

McGoran, C. J. M., Duncan, D. W. & Walden, C. C. 1969. Growth of *Thiobacillus ferrooxidans* on various substrates. *Canadian Journal of Microbiology,* 15**,** 135-138.

Miles, A. A., Misra, S. S. & Irwin, J. O. 1938. The estimation of the bacterial power of the blood. *Journal of Hygiene,* 38**,** 732-749.

Moinier, D., Byrne, D., Amouric, A. & Bonnefoy, V. How the RegBA redox responding system controls iron and sulphur oxidation in *Acidithiobacillus ferrooxidans*. *In:* Guiliani, N., Demergasso, C. S., Quatrini, R., Remonsellez, F., Davis-Belmar, C. S., Levican, G., Parada, P., Barahona, C. & Zale, R., eds. 20th International Biohydrometallurgy Symposium, 2013 Antofagasta, Chile. Advanced Materials Research, 186-189.

Moon, J.-A. H. 1995. *Quantification of biomass in a biooxidation system.* MSc, University of Cape Town.

Muñoz, J. A., Blázquez, M. L., Ballester, A. & González, F. 1995. A study of the bioleaching of a Spanish uranium ore. Part III: Column experiments. *Hydrometallurgy,* 38**,** 79-97.

Murr, L. E. 1980. Theory and practice of copper sulphide leaching in dumps and in-situ. *Minerals Science and Engineering,* 12**,** 121 - 189.

Murr, L. E. & Brierley, J. A. 1978. The use of large-scale test facilities in studies of the role of microorganisms in commercial leaching operations. *In:* Murr, L. E., Torma, A. E. & Brierley, J. A. (eds.) *Metallurgical applications of bacterial leaching and related microbiological phenomena.* New York: Academic Press Inc.

Neuburg, H. J., Castillo, J. A., Herrera, M. N., Wiertz, J. V. & Vargas, T. 1991. A model for the bacterial leaching of copper sulfide ores in pilot-scale columns. *International Journal of Mineral Processing,* 31**,** 247-264.

Norgate, T. & Jahanshahi, S. 2010. Low grade ores - Smelt, leach or concentrate. *Minerals Engineering,* 23**,** 65-73.

Panda, S., Sanjay, K., Sukla, L. B., Pradhan, N., Subbaiah, T., Mishra, B. K., Prasad, M. S. R. & Ray, S. K. 2012. Insights into heap bioleaching of low grade chalcopyrite ores - A pilot scale study. *Hydrometallurgy,* 125-126**,** 157-165.

Pantelis, G. & Ritchie, A. I. M. 1991. Macroscopic transport mechanisms as a rate-limiting factor in dump leaching of pyritic ores. *Applied Mathematical Modelling,* 15**,** 136-143.

Pantelis, G. & Ritchie, A. I. M. 1992. Rate-limiting factors in dump leaching of pyritic ores. *Applied Mathematical Modelling,* 16**,** 553-560.

Petersen, J. & Dixon, D. G. A modelling study of the dynamics of sulphide heap leach processes with a view to improved and novel application. *In:* Lorenzen, L., Bradshaw, D. J., Aldrich, C., Eksteen, J. J., Wright, M. & Thom, E., eds. The XXII International Mineral Processing Congress, 2003 Cape Town, South Africa. South African Institute of Mining and Metallurgy, 1231-1240.

Plumb, J. J., McSweeney, N. J. & Franzmann, P. D. 2008. Growth and activity of pure and mixed bioleaching strains on low grade chalcopyrite ore. *Minerals Engineering,* 21**,** 93-99.

Rossi, G. 1990. *Biohydrometallurgy,* Hamburg, Germany, McGraw-Hill Book Company.

Sand, W. & Gehrke, T. 2006. Extracellular polymeric substances mediate bioleaching/biocorrosion via interfacial processes involving iron (III) ions and acidophilic bacteria. *Research in Microbiology,* 157**,** 49-56.

Soto-Rojo, S., Glonek, G., Soto, P., Demergasso, C. S. & Solomon, P. 2013. A descriptive model for microbial population dynamics in a copper sulphide bioleaching heap with spatial and physicochemical considerations. *In:* Guiliani, N., Demergasso, C. S., Quatrini, R., Remonsellez, F., Davis-Belmar, C. S., Levican, G., Parada, P., Barahona, C. & Zale, R., eds. 20th International Biohydrometallurgy Symposium, 2013 Antofagasta, Chile. Trans Tech Publications, Switzerland: Advanced Materials Research, 233-237.

Soulère, L., Guiliani, N., Queneau, Y., Jerez, C. A. & Doutheau, A. 2008. Molecular insights into quorum sensing in *Acidithiobacillus ferrooxidans* bacteria via molecular modelling of the transcriptional regulator AfeR and of the binding mode of long-chain acyl homoserine lactones. *Journal of Molecular Modelling,* 14**,** 599-606.

Tan, Y., Gannon, J. T., Baveye, P. & Alexander, M. 1994. Transport of bacteria in an aquifer sand: Experiments and model simulations. *Water Resources Research,* 30**,** 3243-3252.

Taylor, S. W. & Jaffé, P. R. 1990. Substrate and biomass transport in a porous medium. *Water Resources Research,* 26**,** 2181-2194.

Tributsch, H. 2001. Direct versus indirect bioleaching. *Hydrometallurgy,* 59**,** 177-185.

Tufenkji, N. 2007. Modeling microbial transport in porous media: Traditional approaches and recent developments. *Advances in Water Resources,* 30**,** 1455-1469.

Tupikina, O. V., Minnaar, S. H., Rautenbach, G. F., Dew, D. W. & Harrison, S. T. L. 2014. Effect of inoculum size on the rates of whole ore colonisation of mesophilic, moderate thermophilic and thermophilic acidophiles. *Hydrometallurgy,* 149**,** 244-251.

Valenzuela, S., Banderas, A., Jerez, C. A. & Guiliani, N. 2007. Cell-Cell communication in bacteria. *In:* Donati, E. R. & Sand, W. (eds.) *Microbial Processing of Metal Sulfides.* AA Dordrecht, The Netherlands: Springer.

van Loosdrecht, M. C. M., Lyklema, J., Norde, W. & Zehnder, A. J. B. 1990. Influence of interfaces on microbial activity. *Microbiological Reviews,* 54**,** 75-87.

869 Wang, S. 2005. Copper leaching from chalcopyrite concentrates. *Journal of the Minerals, Metals and*
870 *Materials Society,* 57**,** 48-51.
871 Watling, H. R. 2006. The bioleaching of sulphide minerals with emphasis on copper sulphides - A
872 review. *Hydrometallurgy,* 84**,** 81-108.
873 Williamson, M. A. & Rimstidt, J. D. 1994. The kinetics and electrochemical rate-determining step of
874 aqueous pyrite oxidation. *Geochimica et Cosmochimica Acta,* 58**,** 5443-5454.
875